World Academy of Science, Engineering and Technology
International Journal of Mechanical and Mechatronics Engineering
Vol:5, No:2, 2011

Study on Plasma Creation and Propagation in a Pulsed Magnetoplasmadynamic Thruster

Tony Schönherr, Kimiya Komurasaki, and Georg Herdrich

Abstract—The performance and the plasma created by a pulsed magnetoplasmadynamic thruster for small satellite application is studied to understand better the ablation and plasma propagation processes occurring during the short-time discharge. The results can be applied to improve the quality of the thruster in terms of efficiency, and to tune the propulsion system to the needs required by the satellite mission. Therefore, plasma measurements with a high-speed camera and induction probes, and performance measurements of mass bit and impulse bit were conducted. Values for current sheet propagation speed, mean exhaust velocity and thrust efficiency were derived from these experimental data. A maximum in current sheet propagation was found by the high-speed camera measurements for a medium energy input and confirmed by the induction probes. A quasilinear tendency between the mass bit and the energy input, the current action integral respectively, was found, as well as a linear tendency between the created impulse and the discharge energy. The highest mean exhaust velocity and thrust efficiency was found for the highest energy input.

Keywords—electric propulsion, low-density plasma, pulsed magnetoplasmadynamic thruster, space engineering.

I. Introduction

THE universities of Stuttgart and Tokyo are collaborating in research and development of an electric propulsion system for application on small satellites of about 200 kg. Two missions, *Perseus* and *Lunar Mission BW1*, of the Stuttgart Small Satellite Program will incorporate this system to serve as the main propulsion device on-board. Intense in-orbit testing is scheduled to prove space readiness. The LEO satellite *Perseus* [1] is planned to comprise one pulsed magnetoplasmadynamic (MPD) thruster named *ADD SIMP-LEX* for a first in-orbit application. An important mission objective is the intense evaluation of the propulsion system in regard to operativeness, compatibility and reliability.

Pulsed MPD thrusters, usually referred to as pulsed plasma thruster (PPT), are promising candidates for usage on board of small satellites due to the robust and simple design and the very low requirements in power consumption. They consist of a capacitor bank, a pair of electrodes, an ignition device and the, usually solid, propellant.

During the short-time discharge of about 10 µs, the electrical energy conserved in the capacitors ablates, dissociates and ionizes the propellant creating a low-density plasma which is then accelerated by Lorentz force eventually generating thrust. The composition and propagation of the plasma strongly depends on the electrical properties of the oscillation circuit of the thruster and their resulting progressions of discharge voltage and current. To investigate the phenomena occurring within the plasma during the discharge and the influence of the thruster properties, high-speed camera observations, measurement of the ablated mass shot and impulse bit and the application of induction probes were used.

Due to imperfect acceleration and phenomena like late-time ablation [2] and particulate emission [3], pulsed MPD thrusters often suffer from low thrust efficiency. A better understanding of the ablation processes, especially the ionization, might yield valuable information to improve the propulsion system in terms of efficiency, thus enabling more payload on the satellite.

T. Schönherr is with the Department of Advanced Energy, The University of Tokyo, 277-8561 Kashiwa, Japan e-mail: schoenherr@al.t.u-tokyo.ac.jp.
K. Komurasaki is with the Department of Advanced Energy, The University of Tokyo, 277-8561 Kashiwa, Japan e-mail: komurasaki@k.u-tokyo.ac.jp.
G. Herdrich is with the Institute of Space Systems, Universität Stuttgart, 70569 Stuttgart, Germany e-mail: herdrich@irs.uni-stuttgart.de.

II. Experimental Setup and Equipment

A. Pulsed MPD thruster

Experiments were conducted using the pulsed MPD thruster called *ADD SIMP-LEX* (ADvanceD Stuttgart Impulsing MagnetoPlasmadynamic thruster for Lunar EXploration) shown in Fig. 1.

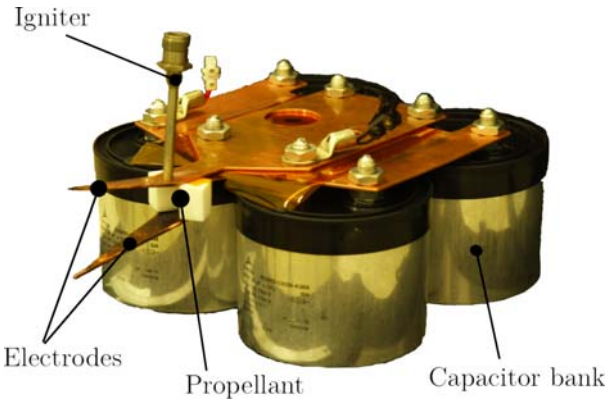

Fig. 1. Setup of ADD SIMP-LEX.

A total capacitance of 80 µF at a maximum voltage of 1300 V allow for a maximum stored energy of 68 J. Solid Teflon™ is used as propellant in the so-called side-fed configuration. The main discharge is triggered by a semiconductor spark plug mounted in the cathode.

After the initial spark, the energy stored in the capacitors is released forming a high-current arc across the surface of the propellant thereby creating a Teflon™ plasma.

Vacuum conditions for near-space environments are achieved by a vacuum chamber with a pump system capable

of a throughput of 2.2 $\times 10^{-3}$ Pa m^3/s at 0.01 Pa. More details about the thruster and the setup were reported earlier [4]–[6].

Discharge voltage and current measurements are conducted in parallel to link the oscillation behavior of the thruster's circuit to the plasma observations [7]. Fig. 2 shows typical discharge progressions of the two properties whereas a picture of the plasma in the visible spectrum is given in Fig. 3.

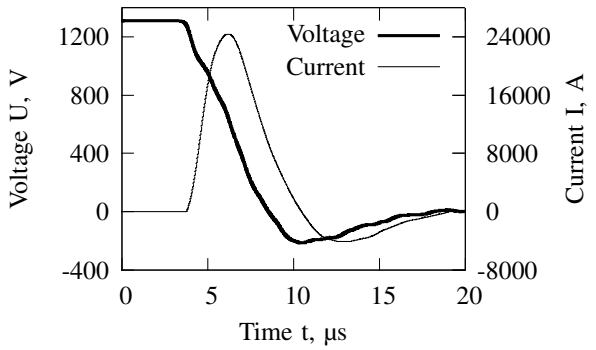

Fig. 2. Typical progression of discharge voltage and current

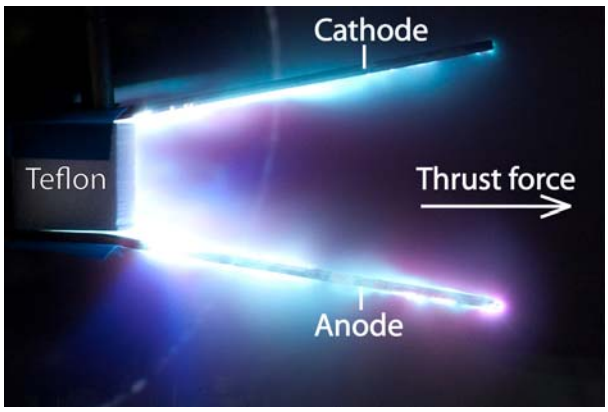

Fig. 3. Exemplary image of the discharge plasma.

B. High-speed camera

To enable an insight into the plasma propagation during the short-time discharge, a DRS Hadland Ltd. Ultra-8 high-speed camera together with a Nikon 85mm f/1.8 lens was applied. With this setup, eight pictures having a resolution of 520 × 520 pixel are taken with a typical exposure time of 100 ns and frame speed of 5 Mfps. As brightness of the emission changes tremendously during the discharge due to the strong variation in discharge current, adjustments in aperture of the lens, and gain of the CCD camera sensor are done to keep brightness almost constant.

The camera is triggered by a photo detector, i.e., recording of the pictures takes place after the initial spark of the igniter. Due to hardware delays, the initial few 100 ns of the discharge cannot be visualized with this system. However, as the view on the plasma creation is blocked by the opaque propellant bars, no information on the actual plasma propagation is lost.

C. Induction probe

The velocity of the propagating current sheet along the thrust axis marked in Fig. 3 is determined by application of two identically-built induction probes. The design is based on previous probes as described, e.g., by Phillips and Turner [8]. 12 windings of a 0.1 mm insulated copper wire around a 1 mm Teflon™ core are connected to a shielded coaxial cable and protected against the plasma by quartz glass tubes. Integration of the signal is done by numerical integration. Perturbation of the plasma by the probes can be considered low, as was investigated by Spanjers and Spores [9].

D. Mass shot measurement

To measure the mass bit ablated by the main discharge, the weight of the Teflon™ propellant bar before and after 500 discharges at a time is recorded. As the expected mass bit would be in the magnitude of tens of µg, a high-precision balance Sartorius R 300 S is used having a resolution of 0.1 mg and a standard deviation of 0.2 mg. As the mass bit might vary with heating of the propellant due to the amount of pulses, each experiment was conducted at a constant pulse frequency of 0.25 Hz to enable comparison. After each experiment, a picture of the ablation and deposition pattern is taken and the propellant bars are cleaned. As Teflon™ adsorbs and absorbs air, the vacuum conditions during the experiment might alter the result of weight measurement. Therefore, the measurement is conducted directly after the experiment, and after 1 h. A standard error is then derived from the differences.

E. Impulse measurement

In order to verify the effect of changes in bank energy on the general performance of the thruster, the induced impulse is measured by a thrust stand that was previously designed to measure low impulses in the order of magnitude of µNs [10].

III. Results and Discussion

A. High-speed camera

Pictures of the propagating plasma were taken for discharge voltages of 500, 900 and 1300 V respectively. 8 frames could be recorded per pulse and were triggered in a time difference of 200 ns. As pulses and triggering of the camera are reproducible, the delay of the camera was adjusted to register the entire plasma phenomenon. Fig. 4 and 5 show a benchmark selection of these plasma pictures. Color was added to the usually black-and-white images for the sake of visibility.

In all three cases, the propagation of the created plasma can be seen during the first few microseconds whereas the brightness and the illumination decrease rapidly after the peak in discharge current and, thus, at 4 to 5 µs after plasma creation most part of the inter-electrode space is not strongly illuminated. For 900 and 1300 V, the thermally accelerated particles can be visibly recognized from 6 µs. After 6 µs, the discharge current changes polarity due to the oscillating behavior of the thruster, and the brightness increases again. However, it is not obvious that electromagnetic acceleration has still a big impact on the particles. Presumably, most part

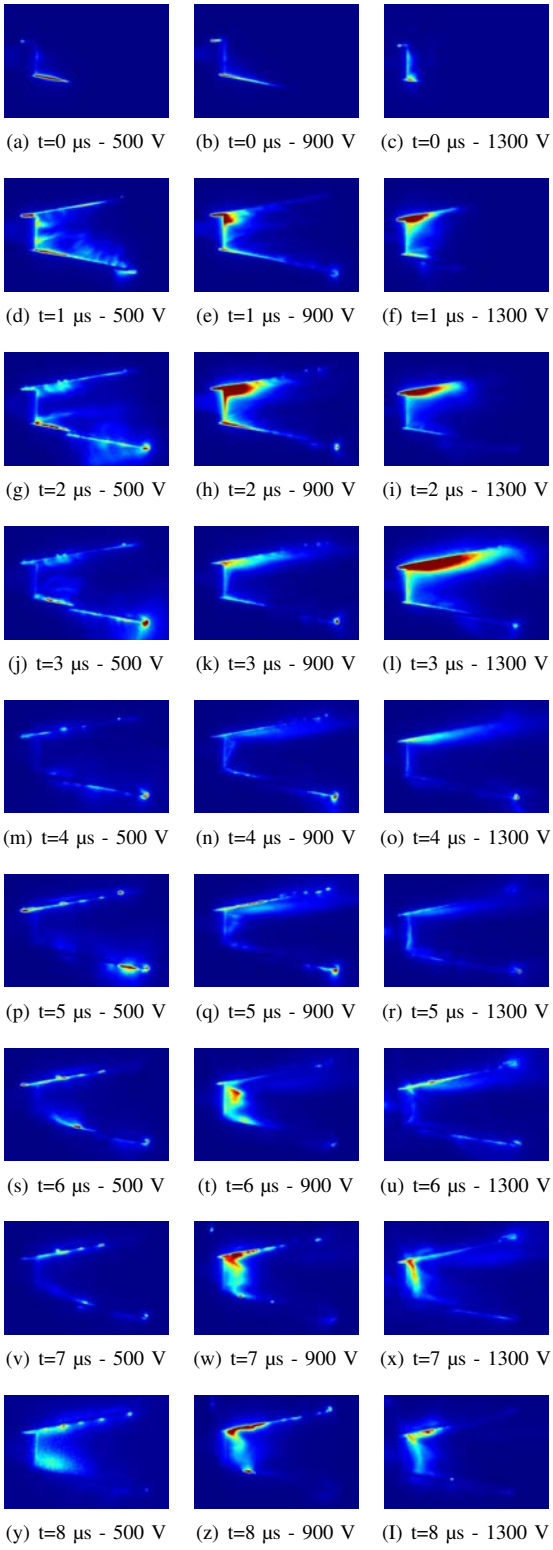

Fig. 4. Pictures captured with high-speed camera at 3 voltage levels.

of the remaining plasma consists of excited neutral atoms and molecules.

The pictures further show clearly a strong plasma canting effect, observed in other thrusters before [11]. The current sheet itself is not distinguishable in the images, however, as

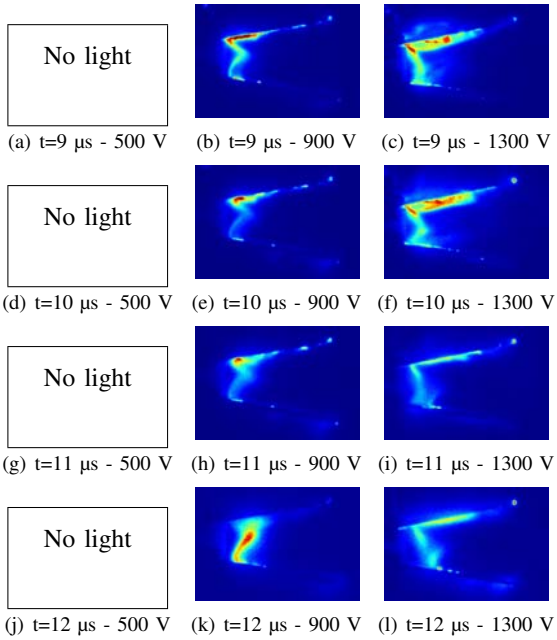

Fig. 5. Pictures captured with high-speed camera at 3 voltage levels (ctd.).

no plasma is created in front of the current sheet, the border of plasma illumination can be estimated as being the current sheet position. As the plasma is not uniform, several points were traced throughout the pictures of the first few microseconds to derive an estimation of the velocity. Fig. 6 shows the results for the tracing within the 500 V images.

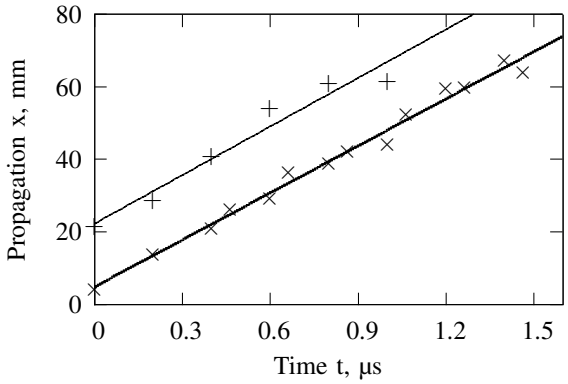

Fig. 6. Propagation positions for different points for 500 V.

From this propagation information a velocity of the plasma, and, hence, the current sheet can be drawn, and the results are summarized in Table I.

TABLE I
CURRENT SHEET PROPAGATION VELOCITIES, IN KM/S

500 V	900 V	1300 V
43.1	55.4	25.7

The configuration using 900 V as a discharge voltage showed the highest velocity in the experiments whereas the highest energy input yielded the lowest current sheet velocity.

The following sections will present more data to explain this phenomenon.

B. Induction probes

The two induction probes were positioned 20 mm downstream of the propellant exit plane, symmetrically away from the center plane of the inter-electrode discharge space. Fig. 7(a) and 7(b) show the setup.

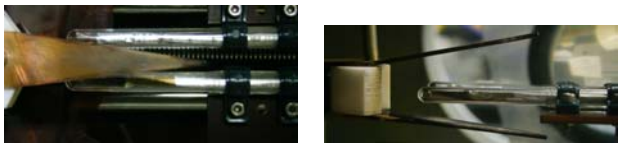

(a) Top view (b) Side view

Fig. 7. Setup of induction probes in parallel configuration.

In this case, the passage of the current sheet and, thus, the evolution of the magnetic field is concurrent. An example of the integrated signal output is plotted in Fig. 8.

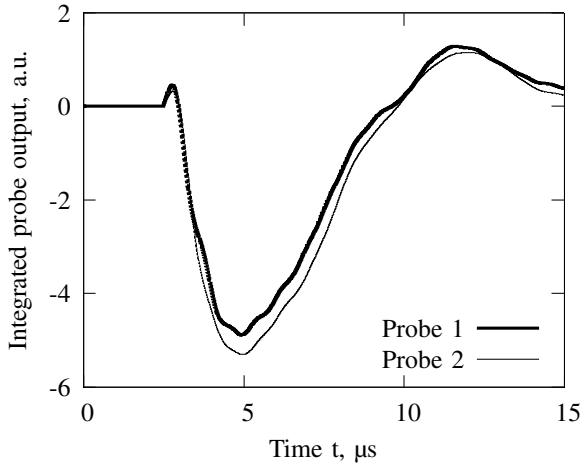

Fig. 8. Integrated probe output for the two parallel-placed induction probes.

The first maximum indicates the approach of the current sheet and thus the raise in magnetic field. The passage reverses the magnetic field causing the signal of the integrated probe output to turn negative and reach a minimum when the magnetic field reaches the maximum. As the plot in Fig. 8 is taken for 1300 V, a second passage of a current sheet is observed forming a maximum in magnetic field. This happens at a time when the electrodes have already changed polarity as the discharge voltage indicates in Fig. 2.

In order to obtain information about the propagation speed of the current sheet, one of the probes was moved another 20 mm downstream, and the signals of the probes were recorded and integrated for different voltages. The setup is shown in Fig. 9 and a typical output is found in Fig. 10.

It is obvious that the maximum amplitude of the magnetic field of probe 2 is smaller as the probe is no longer in the same downstream position as probe 1 and the magnetic field is inhomogeneous throughout the inter-electrode space, but

Fig. 9. Setup of induction probes in shifted configuration.

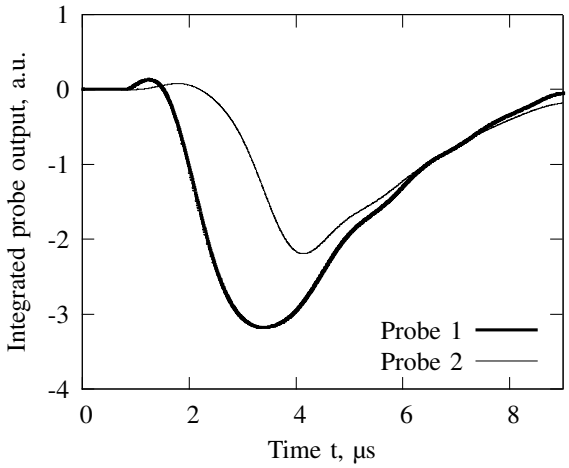

Fig. 10. Integrated probe output for the two shifted induction probes.

clearly the shift in time can be determined from both the intersection and the minimum of the curve, i.e., the maximum magnetic field. The signals of 10 pulses were processed in this way, and the results averaged. Fig. 11 shows the determined velocities for the different voltages, as well as the velocities that were estimated by the high-speed camera (HSC) pictures of section III-A.

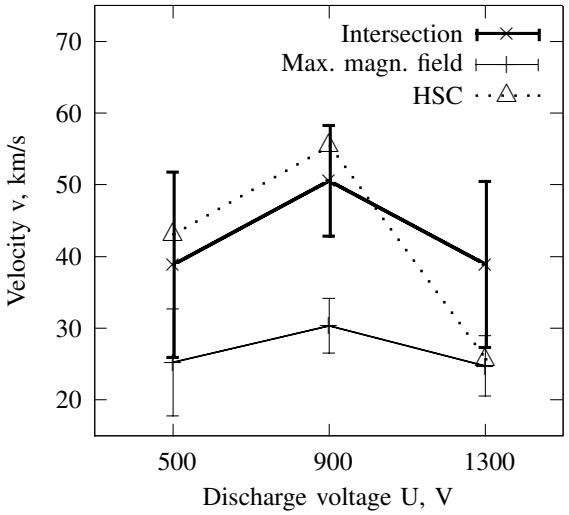

Fig. 11. Estimated velocities from induction probes and high-speed camera.

The data show good accordance with each other, as a maximum in velocity was found at 900 V for all 3 plots. The values for the intersection, which express the velocity

of the current sheet, i.e., the same phenomenon as observed with the high-speed camera, comply well with the values of the latter. Although a certain error due to noise lies within the results, on average the concave progression is visible. For 1300 V, the values of the high-speed camera drop lower than the values of the zero passage which might be linked to the fact that a higher discharge current, and hence, a brighter plasma might defy a precise visualization of the current sheet in the high-speed camera experiments. As the value is close to the value estimated by the maximum magnetic field, the brightness observed and traced in section III-A is then probably the slightly slower plasma following the current sheet.

C. Mass shot measurement

The ablated mass shot was measured for voltages ranging from 500 to the maximum voltage of 1300 V. The results of these experiments against the discharge voltage with a single standard error are plotted in Fig. 12.

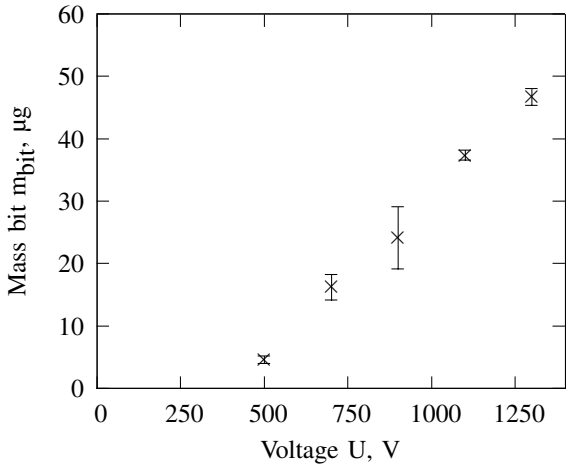

Fig. 12. Measured ablated mass shot for different discharge voltages.

The data indicate that there is a minimum discharge voltage at which mass is no longer ablated between 300 and 400 V. However, experiments showed that the discharge and, hence, the creation of plasma could be triggered down to voltages of 60 V. Plotting the mass bit data against the bank energy $E_0 = \frac{1}{2}C \cdot U^2$ in Fig. 13 yields a linear correlation between the two values. That means, putting more energy into the system directly translates into a linear increase in ablated mass.

However, a higher energy in the system does not directly imply a higher energy density in the discharge space. Due to losses in the resistive parts of the thruster, a better indicator for the direct energy input is the so-called current action integral Ψ and is defined as:

$$\Psi = \int_0^\infty I^2 \, \mathrm{d}t. \tag{1}$$

The values for the current action integral had been determined in a previous study [7]. Fig. 14 presents the linkage between the ablated mass and these values.

It can be seen that for voltages between 500 ($\Psi = 195A^2s$) and 900 V ($\Psi = 644A^2s$) a quasilinear tendency can be

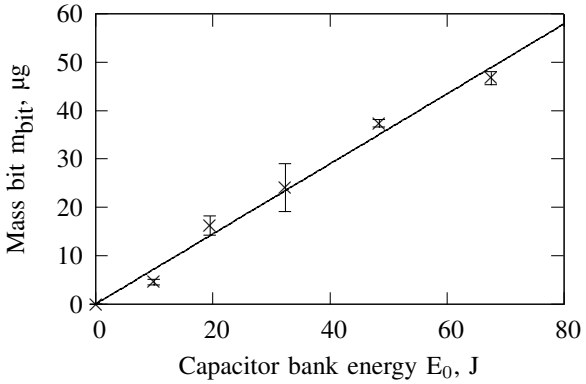

Fig. 13. Measured ablated mass shot against stored bank energy.

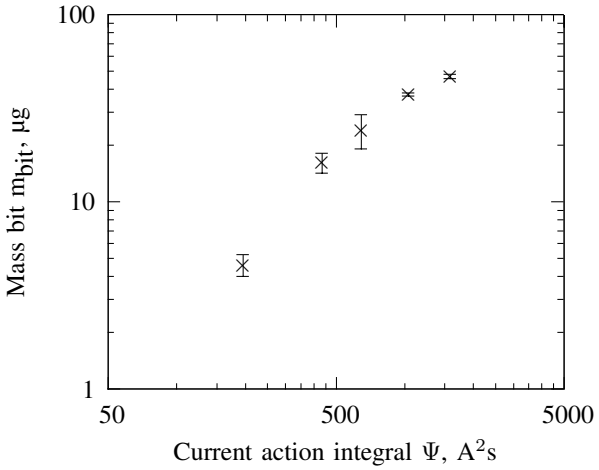

Fig. 14. Measured ablated mass shot against current action integrals.

observed whereas for higher voltages the plot starts to level off. A similar progression had been found by Palumbo and Guman [12] for a different thruster design, indicating that this is a more general property for solid propellant PPT. However, no explanation for this effect was given at that time. To elucidate this phenomenon, pictures of the ablation pattern were recorded for each of the data points, and are displayed in Fig. 15. Only one of the propellant bars is shown with the symmetry plane and the spark plug being on the right side of each picture. The cathode side is at the top, the anode at the bottom respectively.

In case of 500 V, a substantial deposition of carbon (black) and fluorine (yellow) can be observed in the upper left corner, i.e., at the outer cathode side. Depositions indicate that the energy density at this point is not sufficient to easily ablate and ionize material from the surface, but that the discharge arc is concentrated at the center of the discharge space. The cathode side, being the one where the arc is initiated by the spark of the igniter shows a very narrow white ablation pattern whereas the anode side is broader due to the more diffuse nature of the discharge arc. Increasing the voltage at the capacitor bank to 700, and 900 V respectively, narrows the discharge channel of the arc, thereby moving the deposition pattern to the right. A narrower and, thus, more stable discharge arc provides a more

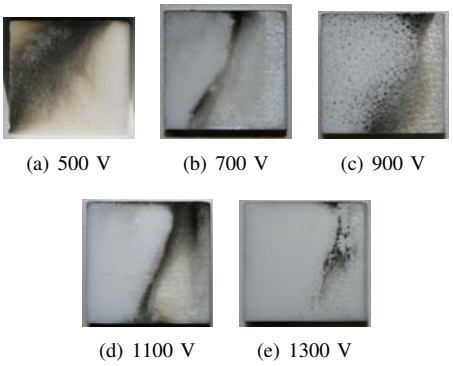

(a) 500 V (b) 700 V (c) 900 V

(d) 1100 V (e) 1300 V

Fig. 15. Ablation patterns of the Teflon™ propellant after 500 discharges.

concentrated magnetic field and a higher ionization rate due to the higher current density and the overall higher energy. This would eventually lead to a higher top speed of the charged particles as was found with the measurements of the high-speed camera and the induction probes in section III-A, and III-B respectively.

An increase beyond 900 V yields a nearly similar deposition pattern with almost no deposition at 1300 V. The discharge arc is, hence, not narrowed any further. As more energy is put into the discharge space, an increased area of the propellant surface is used not only for direct ionizing ablation but also for the often reported late-time ablation due to thermal impact. An increase in usage of propellant surface decreases the current density. So, even though the total energy is increasing and the maximum velocity of the charged particles reduces. However, due to the more homogeneous ablation pattern, a bigger fraction of the ablated mass can benefit from the current density and the induced Lorentz acceleration and, thus, the total thrust is positively affected. Further, a more uniform ablation facilitates the propellant feed for long-time satellite missions.

As the surface of the Teflon™ bar is geometrically limited, the spread of the ablation is restricted causing the flattening of the ablation curve seen in Fig. 14. In this case, deeper layers of propellant need to be ablated consuming more energy, and thus, the total mass bit is reduced.

D. Impulse measurement

Measurements of the impulse bit I_{bit} were conducted in order to verify the effect of the discharge voltage on the thruster performance. 10 measurements were carried out for each voltage level. Together with the mass bit of section III-C, the values for mean exhaust velocity c_e and thrust efficiency η_T can be derived by:

$$c_e = \frac{I_{bit}}{m_{bit}} \qquad (2) \qquad \eta_T = \frac{I_{bit}^2}{2 \cdot m_{bit} \cdot E_0} \qquad (3)$$

Calibration of the impulse balance was challenging by the comparably high weight of the thruster, and a reliable calibration factor could not be determined. However, for the evaluation of the influence, relative changes in the oscillation of the balance are sufficient for discussion. Hence, the measured values are normalized by the impulse bit found for 1300 V. Fig. 16 shows the resulting values with a simple standard error plotted against the bank energy and the current action integral. For both plots, a linear tendency is observed, confirming measurements on other thrusters, e.g., the one of the LES-6 satellite [13].

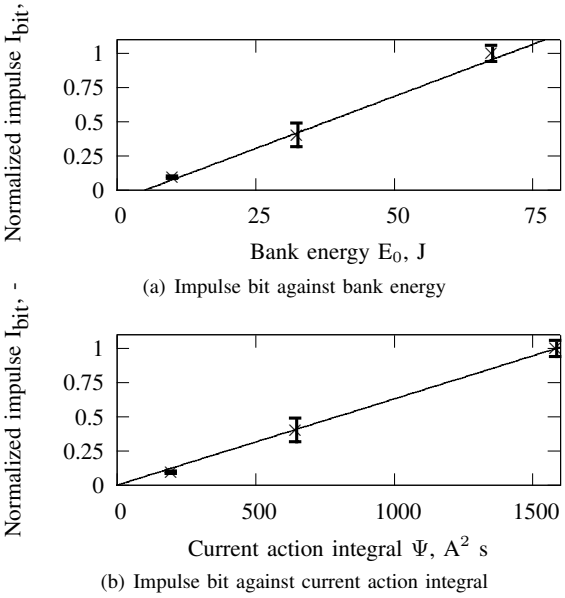

(a) Impulse bit against bank energy

(b) Impulse bit against current action integral

Fig. 16. Normalized impulse bits for different energies.

The impulse bit comprises the electrothermal and the electromagnetic acceleration with the latter being often regarded proportional to the current action integral [14]. As the measured impulse follows a quasilinear tendency, it can be assumed that the electromagnetic acceleration is larger than the electrothermal one by at least one order of magnitude which is the preferable case.

More details about the performance are found in computing the values for the mean exhaust velocity and the thrust efficiency using (2) and (3), again only in relative values. The results and the propagated standard errors are found in Fig. 17(a), and 17(b) respectively.

Although the highest velocity for the current sheet was found for a configuration at 900 V, the mean exhaust velocity does not show the same tendency. As already explained in section III-C, the higher surface consumption during the discharge yields more mass to achieve a high velocity therefore increasing the mean exhaust velocity. As for the thrust efficiency, the values indicate an increase with higher energy levels, but no reliable conclusion about the progression between the low and high energy level can be drawn.

IV. Conclusion

The ablation and plasma propagation within the pulsed magnetoplasmadynamic thruster *ADD SIMP-LEX* was studied thoroughly by application of several measurement methods. An extension of this research will include emission spectroscopic measurements and Fabry-Pérot interferometry. Further, research on a one-capacitor configuration is currently conducted and will extend the understanding of the processes investigated for the four-capacitor configuration.

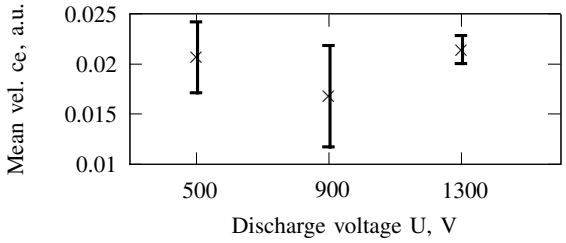

(a) Mean exhaust velocity

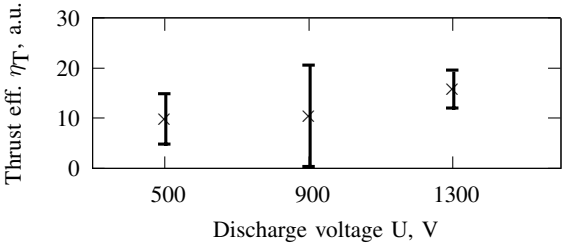

(b) Thrust efficiency

Fig. 17. Performance properties for different discharge voltages.

A maximum current sheet velocity was found for an energy level different to the highest bank energy, but the mean exhaust velocity, as an average of all accelerated particles independent of their charge, crests at maximum energy. Estimations of the degree of ionization and the relative number densities might yield to a full picture of the plasma creation process.

As for the satellite mission, the results suggest the application of the highest energy level to consume the propellant most efficiently. Thermal and lifetime concerns are under investigation at the university in Stuttgart to justify this choice.

The results of these studies can eventually be used to obtain a numerical model suitable for performance prediction and thruster optimization.

ACKNOWLEDGMENT

The authors would like to thank Mr. T. Shimizu for experimental help with the impulse bit measurements. This work is supported by the *Monbukagakusho* scholarship.

REFERENCES

[1] D. Bock, G. Herdrich, M. Lau, T. Schönherr, B. Wollenhaupt, and H.-P. Röser, "Electric propulsion systems for small satellites: The LEO mission Perseus," in *3rd European Conf. for Aero-Space Sciences*, Versailles, France, July 2009.

[2] E. L. Antonsen, R. L. Burton, G. A. Reed, and G. G. Spanjers, "Effects of postpulse surface temperature on micropulsed plasma thruster operation," *J. Propul. Power*, vol. 21, no. 5, pp. 877–883, September-October 2005.

[3] G. G. Spanjers, J. S. Lotspeich, K. A. McFall, and R. E. Spores, "Propellant losses because of particulate emission in a pulsed plasma thruster," *J. Propul. Power*, vol. 14, no. 4, pp. 554–559, July-August 1998.

[4] T. Schönherr, K. Komurasaki, M. Lau, G. Herdrich, H.-P. Röser, S. Yokota, and Y. Arakawa, "Cooperation activities between IRS and the University of Tokyo in the field of pulsed plasma thruster development," in *Proc. 31st IEPC*, Ann Arbor, MI, USA, September 2009.

[5] T. Schönherr, A. Nawaz, M. Lau, D. Petkow, and G. Herdrich, "Review of pulsed plasma thruster development at IRS," in *Trans. JSASS, Aerospace Technology Japan*. JSASS, 2010 (to be published).

[6] A. Nawaz, R. Albertoni, and M. Auweter-Kurtz, "Thrust efficiency optimization of the pulsed plasma thruster SIMP-LEX," *Acta Astronaut.*, vol. 67, no. 3-4, pp. 440–448, August-September 2010.

[7] T. Schönherr, K. Komurasaki, R. Kawashima, Y. Arakawa, and G. Herdrich, "Effect of capacitance on discharge behavior of pulsed plasma thruster," *App. Plasma Sci.*, vol. 18, no. 1, pp. 23–28, June 2010.

[8] R. C. Phillips and E. B. Turner, "Construction and calibration techniques of high frequency magnetic probes," *Rev. Sci. Instrum.*, vol. 36, no. 12, pp. 1822–1825, December 1965.

[9] G. G. Spanjers and R. A. Spores, "PPT research at AFRL: Material probes to measure the magnetic field distribution in a pulsed plasma thruster," in *34th AIAA/ASME/SAE/ASEE JPC*, Cleveland, OH, USA, July 1998.

[10] H. Koizumi, K. Komurasaki, and Y. Arakawa, "Development of thrust stand for low impulse measurement from microthrusters," *Rev. Sci. Instrum.*, vol. 75, no. 10, pp. 3185–3190, Oct. 2004.

[11] T. E. Markusic, J. W. Berkery, and E. Choueiri, "Visualization of current sheet evolution in a pulsed plasma accelerator," *IEEE Trans. Plasma Sci.*, vol. 33, no. 2, pp. 528–529, April 2005.

[12] D. J. Palumbo and W. J. Guman, "Propellant sidefeed-short pulse discharge thruster studies," Fairchild Industries Inc., Farmingdale, NY, USA, Technical Report NASA CR-112035, January 1972.

[13] R. J. Vondra, K. I. Thomassen, and A. Solbes, "Analysis of solid teflon pulsed plasma thruster," *J. Spacecraft Rockets*, vol. 7, no. 12, pp. 1402–1406, December 1970.

[14] D. J. Palumbo and W. J. Guman, "Effects of propellant and electrode geometry on pulsed ablative plasma thruster performance," *J. Spacecraft Rockets*, vol. 13, no. 3, pp. 163–167, March 1976.